Toxicology Letters 295 (2018) 153–161

Contents lists available at ScienceDirect

Toxicology Letters

journal homepage: www.elsevier.com/locate/toxlet

Inhibitory effect of PXR on ammonia-induced hepatocyte autophagy via P53

Linlin Yan[a], Zhanfei Chen[a], Luxi Wu[a], Yongfa Su[a], Xiaoqian Wang[a], Nanhong Tang[a,b,*]

[a] Fujian Institute of Hepatobiliary Surgery, Fujian Medical University Union Hospital, Fuzhou, China
[b] Key Laboratory of Ministry of Education for Gastrointestinal Cancer, Research Center for Molecular Medicine, Fujian Medical University, Fuzhou, China

ARTICLE INFO

Keywords:
Hepatocyte
Autophagy
Ammonia
Pregnane X receptor

ABSTRACT

Pregnane X Receptor (PXR), a nuclear receptor transcription factor, participates in a wide range of physiological activities, but the regulation of ammonia-induced hepatocyte autophagy by PXR is not yet clear. In this study, the levels of down-regulated LC3B-II and up-regulated SQSTM1 were found in ammonia-induced PXR-over-expressing (PXR +) liver cells, but the opposite appeared in PXR-knockdown (PXR −) liver cells. Rifampicin, a PXR-activating agent, elicits a similar effect as PXR + cells. The mechanism analysis reveals that the levels of the energy-sensitive molecule AMPKβ1 and phosphorylated AMPKβ1 (p-AMPKβ1) in PXR − cells are higher than those in control cells, whereas the levels of this molecule in PXR + cells are lower than those in control cells. Two active sites that bind to P53 exist in −253 to −19 at the promoter region of AMPKβ1, and their mutation can reduce the transactivating effect of AMPKβ1 that P53 relies on. A protein interaction also exists between PXR and P53. These findings indicate that PXR is a factor interfering the formation of ammonia-induced hepatocyte autophagy, and its inhibitory effect is achieved when P53 downregulates the expression and activity of AMPKβ1. This conclusion provides an appropriate clinical explanation for hepatotoxicity caused by the inhibitory effect of PXR-activating agent on hepatocyte autophagy.

1. Introduction

Autophagy is a key biological regulatory mechanism of the growth, death, and energy metabolism of eukaryotes (He and Klionsky, 2009). A low level of autophagy is normally maintained in cells, but this level may increase when cells are stimulated by some pressure signals, such as nutrient deficiency, endoplasmic reticulum stress, and other stimuli (Kroemer et al., 2010). The underlying mechanism may generally involve mammalian target of rapamycin (mTOR), which is a key gatekeeper for the regulation of autophagy occurrence and level, and a protein kinase, such as AMP-activated protein kinase (AMPK), which is an energy sensor implicated in cellular autophagy (Mathew et al., 2014; Neufeld, 2010).

Patients suffering from hepatic coma due to an impaired hepatic function are often examined clinically, and this condition is mainly attributed to an increased blood ammonia level (Douglass et al., 2003; Gitlin et al., 1986). In tumor tissues, ammonia accumulation caused by an increased catabolism of glutamine are also observed frequently (Szeliga and Obara-Michlewska, 2009). Ammonia, as a new type of autophagy-inducing agent that triggers autophagy at a low concentration and supports cell survival (Eng and Abraham, 2010), but its mechanism has yet to be fully elaborated. Researches have verified that ammonia-induced autophagy does not rely on changes in mTOR and Unc-51 like autophagy activating kinase (ULK1/2) activities, the signal pathways differ from classical mTOR-ULK1/2 (Cheong et al., 2011; Eng et al., 2010). Another study revealed that the primary driver of ammonia-induced autophagy may be linked to the unfolded protein response (uPR) and the upregulation of AMPK, especially AMPK has an ammonia-specific upregulated phosphorylation (Ser108) on the AMPKβ1 subunit (Harder et al., 2014). These results suggesting that AMPK may be another key factor that drives ammonia-induced autophagy. Hyperammonemia can destroy the mitochondria and tricarboxylic acid cycle and cause a disorder in energy metabolism (Wang et al., 2014b), but a decrease in blood ammonia level can alleviate hepatocyte damage and apoptosis (Gao et al., 2015), implying that autophagy caused by continuous intense ammonia stimulation helps facilitate hepatocyte damage.

The Pregnane X receptor (PXR) is a member of the nuclear receptor family considered to be a major xenobiotic receptor that coordinately regulates the expression of genes encoding drug-metabolizing enzymes and drug transporters, to essentially detoxify and eliminate xenobiotics and endotoxins from the body (Oladimeji and Chen, 2018). As a ligand-activated receptor factor, PXR and Retinoid X Receptor form a heterodimer when ligands, such as medicine, steroid, and bile acid, bind to and activate PXR, thereby regulating the expression of target genes, such as CYP3 A4 and MDR1. Recently, more researches are focused on

* Corresponding author at: Fujian Institute of Hepatobiliary Surgery, Fujian Medical University Union Hospital, No. 29 Xinquan Rd., Fuzhou, Fujian 350001, China.
E-mail address: fztnh@sina.com (N. Tang).

https://doi.org/10.1016/j.toxlet.2018.06.1066
Received 6 April 2018; Received in revised form 30 May 2018; Accepted 12 June 2018
Available online 14 June 2018
0378-4274/

discovering the relationship of PXR in inflammation, energy homeostasis, cell proliferation and carcinogenesis. (Andersen et al., 2011; Wang et al., 2012). In LPS/Ga1N-induced liver damage model, PXR can downregulate the expression of apoptosis-related genes and protect hepatocytes (Wang et al., 2010). However, the influence of PXR on autophagy, especially ammonia-induced hepatocyte autophagy has yet to be reported. This study aimed to investigate the effect of PXR on ammonia-induced autophagy and to elucidate possible mechanisms. We fund that PXR can reduce ammonia-induced hepatocyte autophagy by inhibiting the regulatory effect of p53 transcription factor on AMPK and preliminarily elaborated the influence of PXR, which is a nuclear receptor related to the metabolism of clinical drugs for hepatic coma and other liver diseases, on this process and its molecular mechanism.

2. Materials and methods

2.1. Cell culture and transfection

HL-7702 and BEL-7404 (Shanghai Cell Biology Institute of Chinese Academy of Science, Shanghai, China) were maintained in Dulbecco's modified Eagle medium (DMEM; Life Technologies, Grand island, NY) supplemented with 12% (v/v) foetal bovine serum (FBS, Life Technologies). Cells were plated at a density of 2×10^5 cells/well. DNA transfection was carried out in 24-well plates by use of Lipofectamine 2000 (Invitrogen, Carlsbad, CA), in accordance with the manufacturer's recommendations.

2.2. Treatment protocols and antibodies

Ammonium chloride (NH_4Cl) (A4514, Sigma–Aldrich, St. Louis, MO) was dissolved in DMEM medium and added to a final concentration of 3, 10, or 15 mM for the indicated times. Bafilomycin A1 (B1793, Sigma–Aldrich) was dissolved in DMSO and added to a final concentration of 100 nM for the times indicated. Rifampicin (R3501, Sigma–Aldrich) was dissolved in DMSO medium and added to a final concentration of 10, 20, or 30 mM for the indicated times. The final DMSO concentration is controlled below 0.1%. Antibodies used: LC3B (L7543) from Sigma–Aldrich; SQSTM1 (sc-48402), PXR (sc-48403) and β-actin (sc-47778) from Santa Cruz Biotechnology, Santa Cruz, CA; AMPKα (#5831), AMPKβ1 (#12063), AMPKγ2 (#2536), phospho-AMPKβ1 (#4181), P53 (#2524) and phospho-P53 (#9284) from Cell Signaling Technology, Beverly, MA.

2.3. Generation of PXR-overexpressing (PXR+) and PXR-knockdown (PXR-) stable transfectants

Human cDNA was used as the template to obtain the full length of PXR by PCR for overexpressing, primers used are shown in Table 1. We used the pLent-EF1a-FH-CMV-GP expression system (Vigene, Shandong, China) to construct lentiviruses harboring the PXR. The siRNA targets for PXR (Table 1.) was constructed into pLent-U6-GFP-Puro lentiviral vector (Vigene) for scilence. HL-7702 and BEL-7404 cells were used to infect according to the manufacturer's recommendations. The stable overexpressing and silenced clones were selected after 2 weeks of puromycin (2 μg/ml final concentration) treatment. Detailed method were performed as previously described (Su et al., 2018).

2.4. Western blot assay

Western blot analysis was performed as described previously with slight modifications (Chen et al., 2017). In brief, equivalent amounts of protein were electrophoresed on SDS-polyacrylamide gels and electrophoretic transfer to a polyvinylidene fluoride (PVDF) membrane (Merck Millipore, Darmstadt, Germany). After blocking with 5–7% milk, membranes were incubated with the primary antibody overnight. Finally, the relevant protein was visualized by staining with the appropriate secondary horseradish peroxidaselabeled antibody for 1 h followed by enhanced chemiluminescence. Densitometric analysis of the bands, relative to β-actin, was performed using Image J software (National Institutes of Health).

Table 1
List of oligonucleotides used in this study.[a]

Oligonucleotides	Sequences (5'→3')
AMPKβ1 promoter cloning	
pGL4-1694 (-1527/+167) - F	CCG *CTCGAG* GCCATTCTCCTACTGAACAACT
pGL4-952 (-785/+167) -F	CCG *CTCGAG* CACCCCCGACCCTAATCTGT
pGL4-714 (-547/+167) - F	CCG *CTCGAG* CGCATGAACGGCTCAGATT
pGL4-420 (-253/+167) - F	CCG *CTCGAG* AGTGTCGGTTTATCTTCGC
pGL4-186 (-19/+167) - F	CCG *CTCGAG* GTCCCCGCAGACCCCCAT
pGL4-1694 (-1526/+167) - R	CCC *AAGCTT* GCTCGCACCTTGATTTCCTCG
MDM2 promoter cloning	
Forward	CCG *CTCGAG* GGTTGACTCAGCTTTTCCTCTTG
Reverse	CCC *AAGCTT* GGAAAATGCATGGTTTAAATAGCC
Site-directed mutagenesis	
pGL4-mut1 - F	TTGCGTTCTTGCCGCGG**AG**TGCCTGGGCAGGTAAAGC
pGL4-mut1 - R	CTTTACCTGCCCAGGCA**CT**CCGCGGCAAGAACGCAAG
pGL4-mut2 - F	GCGGCTTGCCTGGG**TG**GGTAAAGCGCGATTG
pGL4-mut2 - R	AATCGCGCTTTACC**CA**CCCAGGCAAGCCGCG
pGL4-mut1 + 2 - F	GCGG**AG**TGCCTGGG**TG**GGTAAAGCGCGATTG
pGL4-mut1 + 2 -R	AATCGCGCTTTACC**CA**CCCAGGCA**CT**CCGCG
ChIP	
AMPKβ1 - F	GTGAAGCGGTTGGGAAAGTG
AMPKβ1 - R	GGAAAGGGACCCTGAGCAAG
MDM2 - F	GGTTGACTCAGCTTTTCCTCTTG
MDM2 - R	GGAAAATGCATGGTTTAAATAGCC
P53 Coding sequence cloning	
Forward	CCG *CTCGAG* GCCACC ATGGAGGAGCCGCAGTCAGAT
Reverse	CCC *AAGCTT* ACAAGAAGTGGAGAATGTCAGT
PXR Coding sequence cloning	
Forward	CCG *CTCGAG* GCCACC CTGGAGGTGAGACCCAAAGA
Reverse	CCC *AAGCTT* CAGCTACCTGTGATGCCGAAC
PXR-siRNA target sequence	CAGGAGCAATTCGCCATTATT
Real-time RT-PCR	
AMPKβ1 - F	CACATCTCCTCCAGGTCATC
AMPKβ1 - R	GCACCATCACTCCATCCTT
GAPDH - F	AGGGCTGCTTTTAACTCTGGT
GAPDH - R	TCTCGCTCCTGGAAGATGGTG

[a] Restriction sites are shown in italics. Mutant bases are underlined.

2.5. Transmission electron microscope (TEM)

BEL-7404 cells were trypsinized and pelleted, suspended and fixed overnight at 4 °C in 2% glutaraldehyde with 1% tannic acid in 0.1 M sodium cacodylate (pH 7.3), and then treated with 1% osmium tetroxide in 0.1 M cacodylate buffer for an additional 1 h. Subsequently, they were stained in 1% uranyl acetate and dehydrated in ethanol. Samples were embedded in epoxy resin, 80-nm sections were cut on a Reighert-Jung Ultra cut E ultramicrotome (Leica Microsystems, Milan, Italy) and picked up on copper grids. After post-stained in uranyl acetate and bismuth subnitrate, the images were observed under a TEM (TEC-NAI 1200, FEI Italia, Milan, Italy).

2.6. AMPKβ1 promoter luciferase constructs

Genomic DNA from normal blood cells, extracted by Genomic DNA

Purification Kit (Promega, Madison, WI), was used as the template for polymerase chain reaction amplification to obtain the putative promoter region of AMPKβ1 (nucleotides -1527 to +167, relative to the translation initiation site) and cloned into pGL4.10-Basic vector (Promega) at *Xho*I and *Hind*III (Thermo Scientific, Waltham, MA) sites to generate pGL4-1694. A series of AMPKβ1 promoter deletion constructs were also made by insertion of the corresponding PCR-generated fragment into the pGL4-Basic plasmid. The pGL4-420 plasmid was used as a template for construction of p53 binding sites mutants (pGL4-mut1, pGL4-mut2 and pGL4-mut1 + 2) through over-lapping extensive PCR. All primers used for amplification are shown in Table 1 and constructs were confirmed by DNA sequencing.

2.7. Dual-luciferase reporter assay

Cells were seeded in triplicate into 24-well plates and co-transfected with the indicated AMPKβ1 promoter reporter vectors, pRL-TK vector (Promega) encoding Renilla luciferase together with the empty vector (pcDNA3.1) or with pcDNA3.1-p53 expression vector. Forty-eight hours after transfection, cells were lysed and their luciferase activities were measured using Dual-Luciferase assay system (Promega) as described previously (Chen et al., 2017).

2.8. Identification of putative transcription factor binding sites

A computer-based search for potential transcription factor binding site motifs was carried out on the TRANSFAC 6.0 (transfac.gbf.de/) professional database by use of TFSEARCH (http://www.cbrc.jp/research/db/TFSEARCH. html) (Meng et al., 2011; Wu et al., 2012), TESS (http://www.cbil.upenn.edu/cgi-bin/tess/tess) programs (Rettino et al., 2009) and TFbind (http://tfbind.hgc.jp/) (Liu et al., 2014).

2.9. Chromatin immunoprecipitation assay (ChIP)

ChIP was performed using Magna-ChIP™ Chromatin Immunoprecipitation kit (Millipore, Temecula, CA) as described previously (Chen et al., 2017). Bound target DNA fractions were analysed by PCR. The primers used are shown in Table 1, which amplified a region that spanned nucleotides −253 to +167 (containing the p53 binding sites) of the AMPKβ1 promoter. The resulting PCR products were electrophoresed on 2% agarose gels and stained with ethidium bromide.

2.10. RNA extraction and real-time RT-PCR analysis

Total RNA was extracted from 7702 cells with TRIzol Reagent (Invitrogen). The reverse transcription reaction was carried out with 2 μg of RNA in a final volume of 20 μl by use of the Transcriptor First Strand cDNA Synthesis Kit (Roche, Mannheim, Germany). Quantitative real-time PCR was performed with the ABI 7500 Real-Time System (Life Technologies) and the Fast Start Universal SYBR Green Master Mix (Roche). The reactions were performed as follows: 50 °C for 2 min, 95 °C for 10 min, and then 40 cycles of 95 °C for 15 s, followed by 60 °C for 1 min. Glyceraldehyde3-phosphate dehydrogenase (GAPDH) served as an internal control. The primers used for GAPDH and AMPKβ1 amplification are shown in Table1. Each sample was analysed in triplicate. The relative expression level of AMPKβ1 was calculated by normalization to the endogenous GAPDH mRNA expression prior to comparative analysis by use of the $2^{-\Delta\Delta Ct}$ method. All procedures followed the manufacturer's instructions.

2.11. Immunoprecipitation assay

Cells (1×10^7) for whole cell lysate were lysed in 800 μl ice cold RIPA buffer and incubate at 4 °C for 20 min. Pellet cellular debris by centrifugation at 10,000 rpm for 10 min at 4 °C. After determining protein concentration using the Bradford assay, 500 μg of the lysate was brought to a final volume of 1 ml with PBS, the remaining part was used as the input group for immunoblot analysis. Lysates were precleared with 1 μg of appropriate control IgG (Beyotime Biotechnology, Shanghai, China) and 20 μl of protein A/G Plus-agarose (Santa Cruz) and kept on a rotator for 1 h at 4 °C. Lysates were centrifuged (2500 rpm for 5 min at 4 °C) and 2 μg of P53 antibody or corresponding IgG was added to the precleared lysates and incubate at 4 °C on a rotating device for 3–5 h. Following incubation, 30 μl of protein A/G Plus-agarose was added to each tube and kept on a rotator overnight at 4 °C. Lysates were then centrifuged (2500 rpm for 5 min at 4 °C). The pellet fractions were washed 4 times with PBS and then resuspended in 20 μl of 1 × loading buffer. Samples were immunoblotted with the appropriate antibody as indicated in the figures.

2.12. Statistical analysis

Each cellular experimental group was repeated for at least three times. The data are expressed as the mean ± SD calculated by GraphPad Prism or SPSS. For multiple comparisons, analysis of variance (ANOVA) followed by Tukey post hoc test was performed. The results were considered statistically significant when $P < 0.05$. All statistical analyses were performed with GraphPad Prism Version 7 (GraphPad Software Inc., SanDiego, CA) and SPSS package (SPSS Inc., Version 13.0.1 for Windows Chicago, IL).

3. Results

3.1. PXR overexpression interferes with ammonia-induced hepatocyte autophagy

To explore the influence of PXR on ammonia-induced hepatocyte autophagy, we established PXR-overexpressing or knockdown HL-7702 and BEL-7404 liver cell lines (upper right insert in Fig. 1A). WT was used as a control group, and three different ammonia concentrations were set to examine the cells for 12 h. 1) In Fig. 1A, the levels of down-regulated LC3B-II and up-regulated SQSTM1 were showed in ammonia-induced PXR+ liver cells, whereas the contrary phenomenon appeared in PXR− cells. 2) The exclusion test is shown in Fig. 1B. In bafilomycin A1 treatment, the LC3B-II level in PXR+ cells is similar to or slightly lower than that of WT cells, but LC3B-II accumulates in PXR− cells, indicating that the decreased LC3B-II expression in PXR+ cells is a result of the reduced autophagy induction, not of excessive autophagic flux. 3) The TEM results (Fig. 1C) also reveal that the number of the formed BEL-7404/PXR autophagic vacuoles/autolysosomes is much more than that of WT after 12 h of treatment with 10 mM ammonia, and this observation is accompanied by active lysosome formation. 4) We further observed whether the PXR-activating agent rifampicin elicits a similar effect. Notably, as the rifampicin concentration increases, the LC3B-II level declines gradually and accompanied by the increase of SQSTM1 (Fig. 1D). These results suggest that PXR is the factor that interferes with ammonia-induced hepatocyte autophagy.

3.2. Regulatory effect of PXR on ammonia-induced AMPKβ1

The energy-sensitive molecule AMPK participates in ammonia-induced autophagy (Harder et al., 2014). AMPK is composed of α, β, and γ subunits, whose distribution in the body differs. We analyzed the correlation of the three subunits and ammonia-induced hepatocyte autophagy. In Fig. 2A, the AMPKβ1 expression increases as the ammonia concentration increases, but the α and γ expression does not change at different ammonia concentrations. In the PXR− group, the expression of AMPKβ1 is higher than that of the WT control group, but opposite result is observed in the PXR+ test group. This phenomenon tends to be much more significant in an environment with 10 mM ammonia than in an environment without ammonia. The

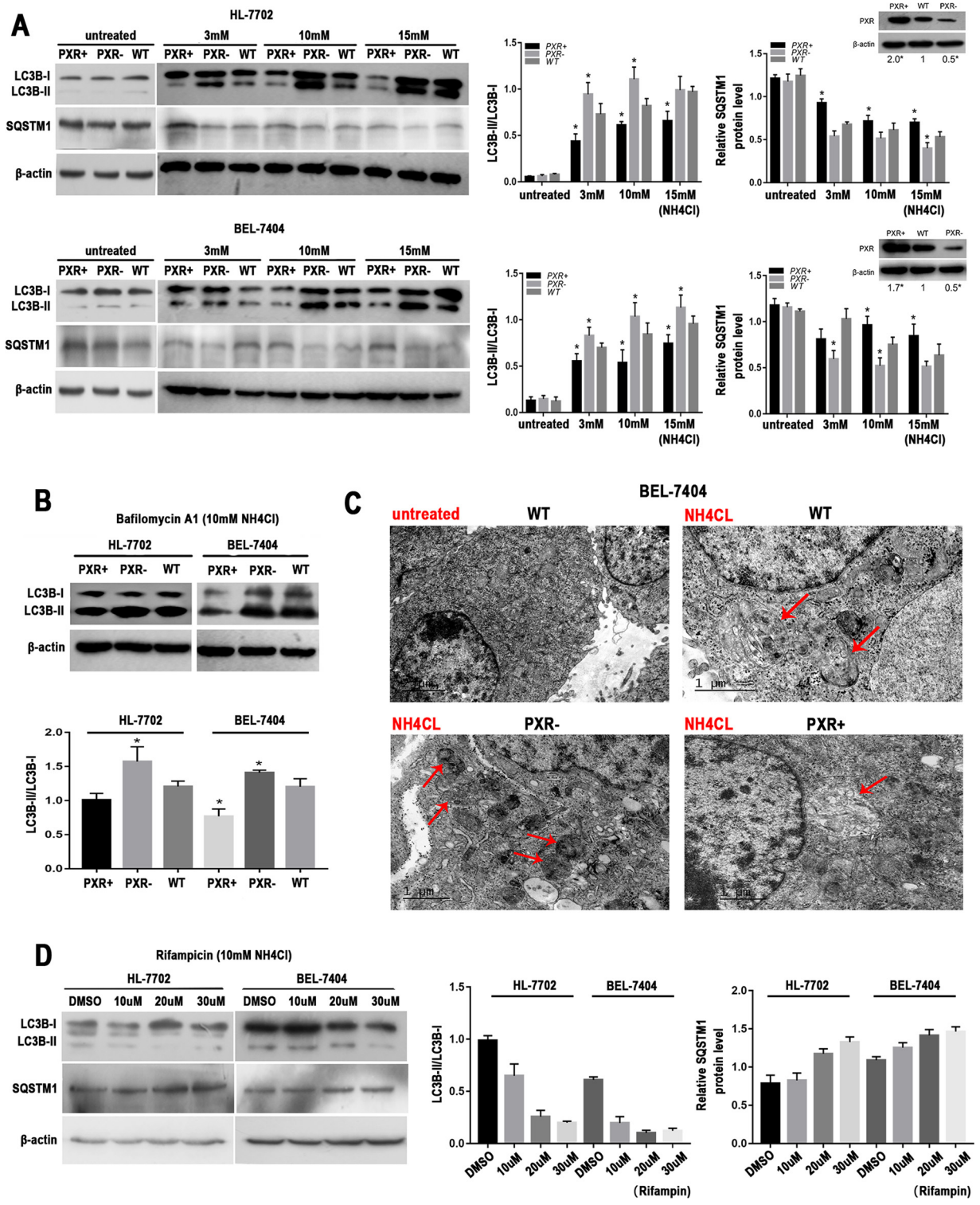

Fig. 1. PXR interferes with ammonia-induced hepatocyte autophagy. (A) Representative immunoblots for LC3B and SQSTM1 expression. The HL-7702 and BEL-7404 cells (WT), and their stable overexpressing or knockdown of PXR (PXR + and PXR-) cells were either untreated, or treated 3, 10 and 15 mM with NH_4Cl for 12 h. The densitometry data were normalized to β-actin. *$P < 0.05$ versus WT cells (n = 3). (B) Representative immunoblots for LC3B in the exclusion test. The HL-7702 and BEL-7404 cells (WT), and their PXR + or PXR- cells were treated with 100 nM bafilomycin A1 for 12 h in combination with 10 mM NH_4Cl. The densitometry data were normalized to β-actin. *$P < 0.05$ versus WT cells (n = 3). (C) Detection of autophagosome formation by TEM. BEL-7404 cells (WT, PXR- and PXR +) were treated with 10 mM NH_4Cl for 12 h. The red arrowheads indicate the autolysosomes/autophagic lysosomes in the cytoplasm. (D) Representative immunoblots for LC3B and SQSTM1 after activation of PXR. HL-7702 and BEL-7404 cells were treated with 10 mM NH_4Cl in combination with 10, 20 and 30 μM rifampicin for 24 h. The densitometry data were normalized to β-actin. *$P < 0.05$ versus WT cells (n = 3) (For interpretation of the references to color in this figure legend, the reader is referred to the web version of this article).

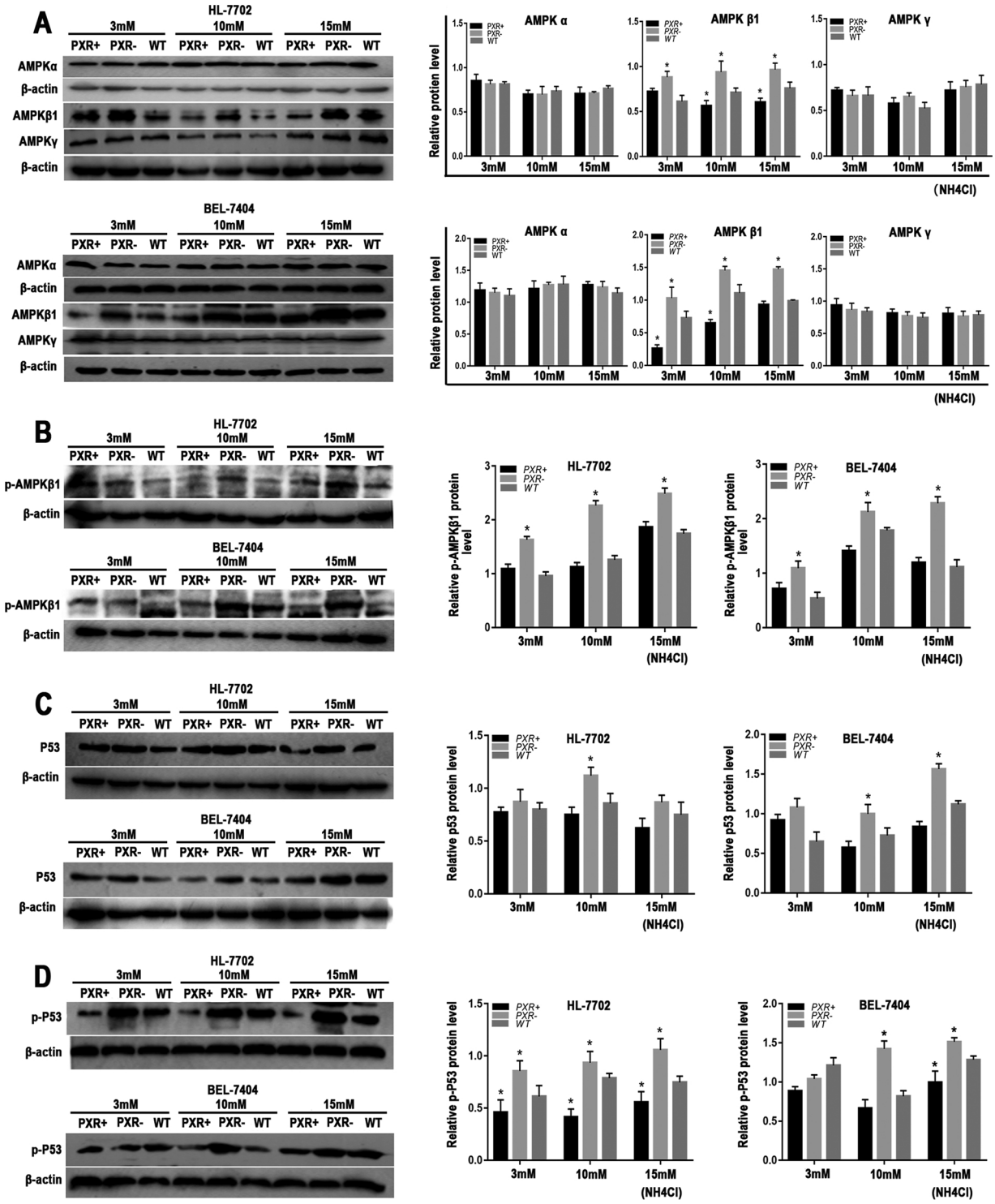

Fig. 2. PXR reduces the expression of AMPKβ1 and P53. Representative immunoblots for (A) AMPK submits (α, β1, and γ), (B) phospho-AMPKβ1 (p-AMPKβ1), (C) P53 and (D) phospho-P53 (p-P53). The HL-7702 and BEL-7404 cells (WT), and their PXR + or PXR- cells were treated with 3, 10 and 15 mM with NH_4Cl for 12 h. The densitometry data were normalized to β-actin. $^*P < 0.05$ versus WT cells (n = 3).

phosphorylated AMPKβ1 (p-AMPKβ1) level shows a similar trend, that is, the AMPKβ1 phosphorylation level increases significantly in the PXR− test group (Fig. 2B). These findings confirm that PXR can downregulate the expression of AMPKβ1 and affect its activation level in an environment with a high ammonia concentration.

We further analyzed the regulatory mechanism of PXR on AMPKβ1. Previous studies demonstrated that ammonia can activate P53 (Panickar et al., 2009), but Feng confirmed that the potential binding site of P53 exists in the promoter of the AMPKβ1 subunit, indicating that P53 may be implicated in ammonia-induced AMPK activation (Feng et al., 2007). P53 is known as one of the molecules that regulate the cell growth cycle and participate in removing cells that are beyond repair and in assisting cells to deal with DNA lesion, metabolic stress, oxidative stress, and other adverse conditions (Maddocks et al., 2013). We investigated the expression level of ammonia-induced hepatocyte P53 and p-P53 levels. The results demonstrate the expression and

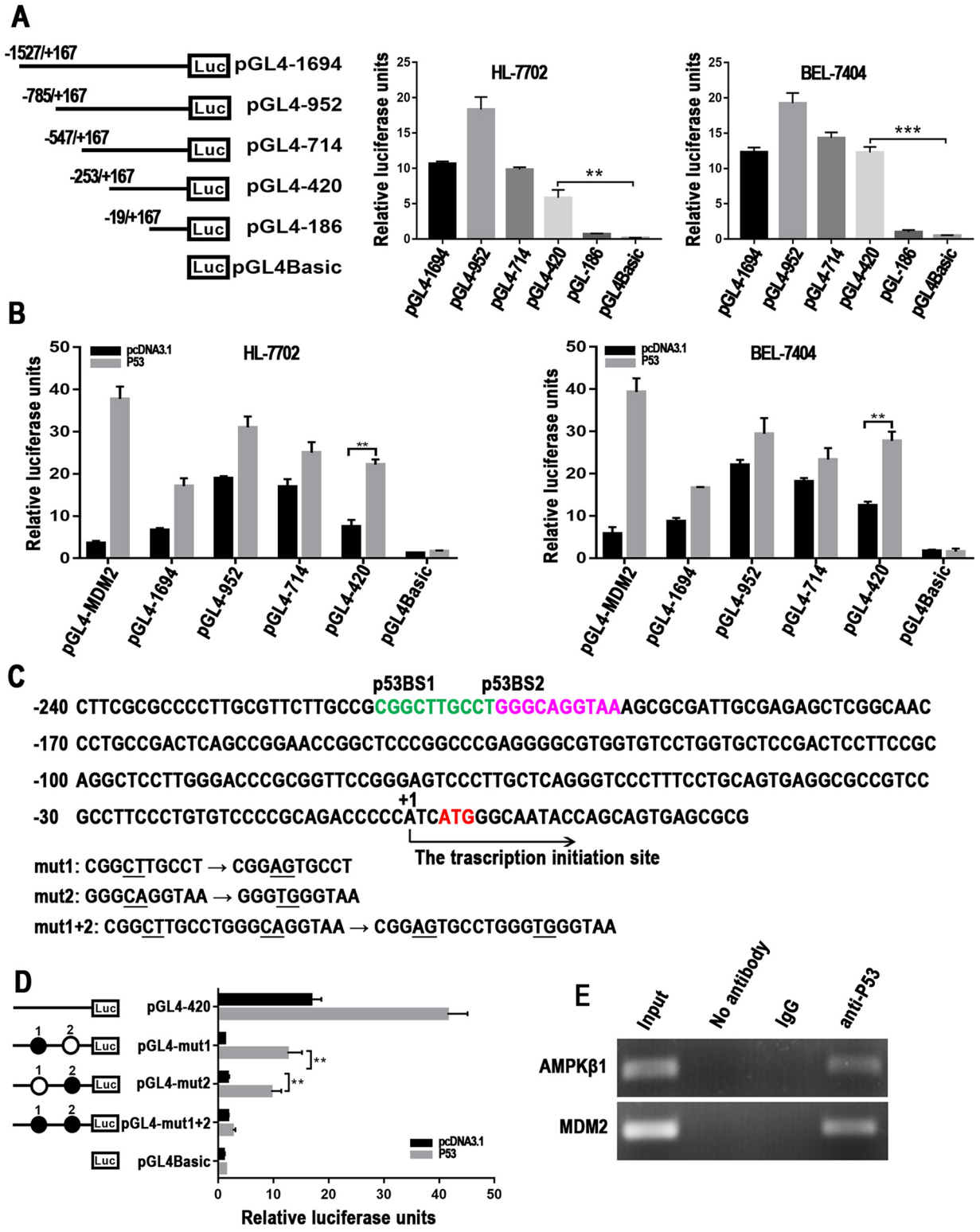

Fig. 3. The regulatory effect of P53 on AMPKβ1 promoter transcription. (A) The activity analysis of AMPKβ1 promoter. HL-7702 and BEL-7404 cells were co-transfected with pRL-TK (50 ng) and each of the AMPKβ1 promoter constructs (reporter plasmid) 1 μg. Luciferase activities were measured 48 h after transfection, and the plasmid pGL4-2086 served as the negative control. (B) Overexpression of P53 enhances AMPKβ1 promoter activity. Each of promoter constructs (500 ng) were co-transfected with p53 (500 ng) in HL-7702 and BEL-7404 cells, pcDNA3.1 vector was used as the negative control. After 48 h for luciferase activity assay. (C) Analysis of potential P53 binding sites in the AMPKβ1 promoter core region. The positions relative to the major AMPKβ1 transcription start site (+1) are indicated. And the mutation sides were indicated at P53 binding sites (P53-BS1 and P53-BS2). (D) Effect of P53 binding site mutations on AMPKβ1 promoter activity. The mutant pGL4-420 promoter constructs (500 ng) was cotransfected into HL-7702 cells with P53 expression plasmid (500 ng) and pcDNA3.1 vector was used as the negative control. Luciferase activity was measured 48 h after transfection. (E) ChIP assay. After immunoprecipitation of chromatin from HL-7702 cells with anti-P53 antibody, total DNA (Input DNA, 2%) and immunoprecipitation samples were amplified by PCR using specific primers, P53 target promoter MDM2 served as a positive control. The data were expressed as the mean ± SD of three separate experiments. $^{**}P < 0.01$, $^{***}P < 0.001$.

activation of the changes in P53 and the specific increase in the ammonia concentration (Figs. 2C, 2D). And we also found that after PXR silence, the P53 level is higher than that of the WT group. The results suggested that the interaction of P53 with PXR in the hepatocyte with a high ammonia concentration may mediate AMPKβ1 expression and autophagy.

3.3. Analysis of a P53 binding site in the AMPKβ1 promoter

We examined the AMPKβ1 promoter to determine whether P53 can directly transactivate AMPKβ1. We intercepted the 1527 bp at the upstream of the AMPKβ1 transcription start site and the first exon genetic sequence and established multiple luciferase report plasmids of the AMPKβ1 promoter based on the analysis results of the prediction software for the promoter binding sites. The results show that the pGL4-420 (−253 to +167) fragment is characterized by a strong promoter activity compared with that of the no-load pGL4.10 control group, but pGL4-186 (−19 to +167) fails to drive luciferase gene expression, predicting that the active region of the AMPKβ1 promoter is probably located at −253 to −19 of the AMPKβ1 gene (Fig. 3A).

We used a P53 expression vector and various promoter reporter vectors in cell co-transfection and selected the MDM2 promoter reporter vector with the P53 target site as the positive control group. Fig. 3B reveals that the P53 expression can significantly enhance the influence of the AMPKβ1 promoter in inducing the expression of luciferase reporter genes, including pGL4-1694, pGL4-952, pGL4-714, and pGL4-420. To verify whether the transactivation of P53 on AMPKβ1 relies on P53 binding, we selected two optimum P53 binding sites (P53-BS1 and P53-BS2) at the 253 to −19 segment based on the prediction results of the software, established a mutant plasmid (Fig. 3C), and combined it with the P53 expression plasmid for the co-transfection of HL-7702 cells. Fig. 3D shows that the sequence changes in two binding sites, namely, P53-BS1 and P53-BS2, can reduce AMPKβ1 transactivation that P53 relies on, but the simultaneous mutation of the two sites can significantly destroy the transcriptional activity of P53. We observed that the two predicted sites are the binding sites of the same P53 because they are spatially adjacent to each other. The specific ChIP verification results through PCR amplification (Fig. 3E) suggest that the P53 antibody can effectively collect the chromatin fragment containing the binding sites P53-BS1 and P53-BS2 in AMPKβ1 (−253 to −19). However, the DNA fragment is detected neither in the ordinary homologous IgG control group nor in the no-antibody control group.

3.4. Interaction of PXR and P53 affects the AMPKβ1 expression

Based on the above results, we further analyzed the influence of P53 and PXR expression on pGL4-420 luciferase driving activity to identify the influencing mechanism of PXR on AMPKβ1 expression. The results (Fig. 4A) reveal no difference in the effect of PXR expression on the enhancement of the activity of AMPKβ1 promoter to drive luciferase genes in the pcDNA3.1 control group, but PXR can downregulate the activating effect of P53 on this segment, confirming that PXR elicits an inhibitory effect on the P53 transcriptional activity. The q-PCR test results show that the AMPKβ1 expression in ammonia-stimulated PXR− cell strains is much higher than that of the WT group (Fig. 4B), and these findings are consistent with Western blot results. Co-IP analysis results (Fig. 4C) suggest that the PXR protein can be effectively enriched after P53 antiserum immunoprecipitation is performed, and this observation is different from that of the negative control. These findings reveal that PXR can exert an inhibitory effect on P53 through a protein–protein interaction with P53.

4. Discussion

As a protective mechanism of eukaryotes in external or internal stimulation, autophagy is generally good for cell survival in adverse environments. Ammonia, as a potential toxic byproduct in amino acid catabolism, plays an important role in inducing autophagy and facilitating cell survival (Coltart et al., 2013; Tranah et al., 2013). Therefore, relevant cytological effects should be explored. After verifying that hepatocytes respond to ammonia stimulation by upregulating autophagy, we further analyzed the influence of ammonia on the AMPK and P53 expression and activity and found that AMPK β1 and P53 activation participates in stress reaction. Sites exist in the −253 to −19 segment of the AMPK promoter for the P53 binding and promotion of its expression. Our results suggest that AMPK is influenced directly by P53 transactivation. Thus, P53 activation facilitates the expression and activation of the autophagy-related gene AMPK as induced by ammonia and plays an important role in the succeeding autophagy.

PXR is well known as a ligand-dependent transcription factor, regulates many biological events by inducing gene transcription (Billas and Moras, 2013). There are evidences that PXR is an apoptotic regulator that promotes the malignant phenotype of cancer. In human colon cancer cells, PXR-mediated deoxycholic acid resistance was associated with up-regulation of multiple antiapoptotic genes, including BAG3, BIRC2, and MCL-1, and down-regulation of proapoptotic genes, such as BAK1 and TP53/p53 (Zhou et al., 2008). In this study, we also found that the expression of P53 and AMPK increased after PXR knockdown. In addition, PXR can also interact directly with transcription factors and inhibit its function (Kodama and Negishi, 2013). So we examined the effect of PXR on the transcriptional activity of p53, notably, we found that PXR can inhibit ammonia-induced autophagy in hepatocytes and is achieved through P53. The results showed that overexpression of PXR can inhibit the transcriptional activity of P53 and inhibit the expression of downstream AMPK. The protein–protein interaction between PXR and P53 may be a mechanism by which PXR exerts its inhibitory effect. This observation is consistent with the findings of D. Robbins et al., who demonstrated that PXR inhibits the transcriptional activity of P53 by interfering with the binding of p53 to a target gene (Robbins et al., 2016). Numerous clinical and therapeutic drugs are PXR ligands, so the influence of PXR on cell stress and apoptosis is essential for disease progression. This study has explained the influencing mechanism of PXR on cell fate in terms of autophagy.

Some studies have revealed that excessively upregulated autophagy can result in hepatocyte damage (Schneider and Cuervo, 2014; Sridhar et al., 2012), but our study demonstrates that the PXR-activating agent can inhibit ammonia-induced autophagy, undermine the self-protection of cells through autophagy, and cause hepatocyte damage. This observation helps explain some clinical drug-induced hepatotoxicity, for instance, the PXR-activating agent often results in hepatotoxicity when it is used alone or in combination with other chemotherapeutic drugs for treatment (Li et al., 2013). In addition, related studies of autophagy and PXR indicated that autophagy inducer sulforaphane can inhibited the expression and also activity of PXR (Wang et al., 2014a). However, differences in the expression of PXR in tissue species may also led to the tissue specificity of the biological effects produced by rifampicin. In BV2 cells, rifampicin promotes autophagy and alleviates inflammatory lesions (Liang et al., 2017). Therefore, liver injury induced by the sole application of this agent or its combination with other chemotherapeutic drugs should be further described. A wide range of lipophilic chemotherapeutic drugs can work as a ligand to activate PXR, because PXR ligand overlaps with the metabolic substrates of its target gene (Prakash et al., 2015). As a result, the multidrug resistance spectrum related to PXR is wide. The potential influence of the PXR-activating agent on the metabolism of various substances, such as carbohydrates and lipids (Kodama and Negishi, 2013; Rysä et al., 2013), and the consequences of its inhibitory effect on hepatocyte autophagy should be considered if this agent would be recommended for long-term use.

Therefore, this test can help demonstrate that the clinical use of the PXR-activating agent or its combination with other drugs may exacerbate hepatotoxicity for the treatment of liver cancer or liver cirrhosis and can also serve as a theoretical and experimental basis for the

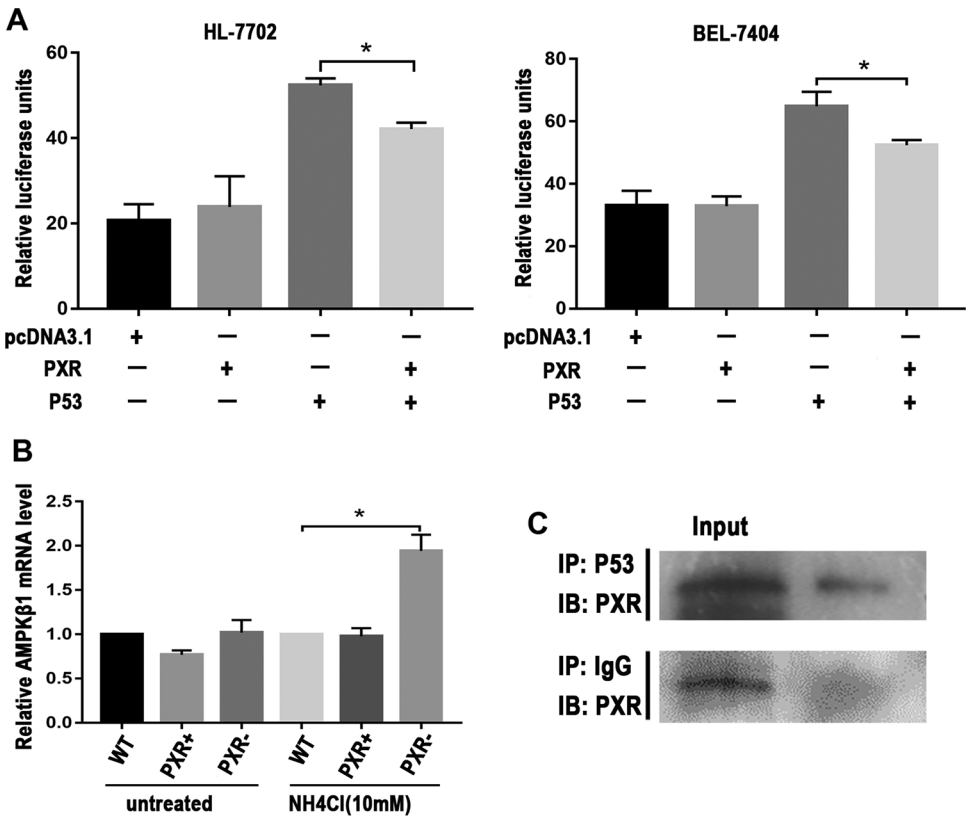

Fig. 4. PXR interacts with P53 to reduce AMPKβ1 mRNA expression. (A) PXR expression inhibits P53 transcriptional activity of AMPKβ1. The fluorescent reporter vector pGL4-420 (500 ng), P53 expression plasmid and/or PXR expression plasmid (250 ng/250 ng) were co-transfected into HL-7702 cells and BEL-7404, pcDNA3.1 vector as the control, the total amount of plasmid DNA controlled to 1 μg. As a negative control, luciferase activity was measured 48 h after transfection. (B) PXR expression inhibits ammonia-induced AMPKβ1 mRNA levels. After treated with ammonia (10 mM) for 12 h, GAPDH-normalized AMPKβ1 mRNA was detected by qRT-PCR in HL-7702 WT, PXR-, PXR + cells. Relative mRNA levels were obtained compared to the wild-type group (set to 1). (C) Interaction between PXR and P53. Cellular extracts were immunoprecipitated with either anti-P53 antibody or anti-rabbit IgG and immunoblotted with an anti-PXR. PXR expression was also determined in the input (first panel). The data were expressed as the mean ± SD of three separate experiments. *$P < 0.05$.

selection of future preventive measures.

Conflict of interest

The authors have no conflicts of interest to declare.

Acknowledgments

This work was supported by the National Natural Science Foundation of China (81470872), the Scientific and Technological Innovation Foundation of Fujian province (2017Y9100) and the Construction Project of National Key Clinical Subject of General Surgery. The authors would like to thank Linying Zhou from the Laboratory of Electron Microscopy, Fujian Medical University, for technical support of Transmission Electron Microscope.

References

Andersen, V., Christensen, J., Ernst, A., Jacobsen, B.A., Tjonneland, A., Krarup, H.B., Vogel, U., 2011. Polymorphisms in NF-kappaB, PXR, LXR, PPARgamma and risk of inflammatory bowel disease. World J. Gastroenterol. 17, 197–206.

Billas, I., Moras, D., 2013. Allosteric controls of nuclear receptor function in the regulation of transcription. J. Mol. Biol. 425, 2317–2329.

Chen, Z., Tang, N., Wang, X., Chen, Y., 2017. The activity of the carbamoyl phosphate synthase 1 promoter in human liver-derived cells is dependent on hepatocyte nuclear factor 3-beta. J. Cell. Mol. Med. 21, 2036–2045.

Cheong, H., Lindsten, T., Wu, J., Lu, C., Thompson, C.B., 2011. Ammonia-induced autophagy is independent of ULK1/ULK2 kinases. Proc. Natl. Acad. Sci. U. S. A. 108, 11121–11126.

Coltart, I., Tranah, T.H., Shawcross, D.L., 2013. Inflammation and hepatic encephalopathy. Arch. Biochem. Biophys. 536, 189–196.

Douglass, A., Al Mardini, H., Record, C.O., 2003. Oral tryptophan challenge studies in cirrhotic patients: no evidence of neuropsychiatric changes. Metab. Brain Dis. 18, 179–186.

Eng, C.H., Abraham, R.T., 2010. Glutaminolysis yields a metabolic by-product that stimulates autophagy. Autophagy 6, 968–970.

Eng, C.H., Yu, K., Lucas, J., White, E., Abraham, R.T., 2010. Ammonia derived from glutaminolysis is a diffusible regulator of autophagy. Sci. Signal. 3, ra31.

Feng, Z., Hu, W., de Stanchina, E., Teresky, A.K., Jin, S., Lowe, S., Levine, A.J., 2007. The regulation of AMPK beta1, TSC2, and PTEN expression by p53: stress, cell and tissue specificity, and the role of these gene products in modulating the IGF-1-AKT-mTOR pathways. Cancer Res. 67, 3043–3053.

Gao, G., Yu, Z., Yan, J., Li, J., Shen, S., Jia, B., Guan, K., Gao, X., Kan, Q., 2015. Lowering blood ammonia prevents hepatocyte injury and apoptosis. Int. J. Clin. Exp. Med. 8, 12347–12355.

Gitlin, N., Lewis, D.C., Hinkley, L., 1986. The diagnosis and prevalence of subclinical hepatic encephalopathy in apparently healthy, ambulant, non-shunted patients with cirrhosis. J. Hepatol. 3, 75–82.

Harder, L.M., Bunkenborg, J., Andersen, J.S., 2014. Inducing autophagy: a comparative phosphoproteomic study of the cellular response to ammonia and rapamycin. Autophagy 10, 339–355.

He, C., Klionsky, D.J., 2009. Regulation mechanisms and signaling pathways of autophagy. Annu. Rev. Genet. 43, 67–93.

Kodama, S., Negishi, M., 2013. PXR cross-talks with internal and external signals in physiological and pathophysiological responses. Drug Metab. Rev. 45, 300–310.

Kroemer, G., Marino, G., Levine, B., 2010. Autophagy and the integrated stress response. Mol. Cell 40, 280–293.

Li, F., Lu, J., Cheng, J., Wang, L., Matsubara, T., Csanaky, I.L., Klaassen, C.D., Gonzalez, F.J., Ma, X., 2013. Human PXR modulates hepatotoxicity associated with rifampicin and isoniazid co-therapy. Nat. Med. 19, 418–420.

Liang, Y., Zhou, T., Chen, Y., Lin, D., Jing, X., Peng, S., Zheng, D., Zeng, Z., Lei, M., Wu, X., Huang, K., Yang, L., Xiao, S., Liu, J., Tao, E., 2017. Rifampicin inhibits rotenone-induced microglial inflammation via enhancement of autophagy. Neurotoxicology 63, 137–145.

Liu, C., Chen, S., Wang, X., Chen, Y., Tang, N., 2014. 15d-PGJ(2) decreases PGE(2) synthesis in HBx-positive liver cells by interfering EGR1 binding to mPGES-1 promoter. Biochem. Pharmacol. 91, 337–347.

Maddocks, O.D., Berkers, C.R., Mason, S.M., Zheng, L., Blyth, K., Gottlieb, E., Vousden, K.H., 2013. Serine starvation induces stress and p53-dependent metabolic remodelling in cancer cells. Nature 493, 542–546.

Mathew, T.S., Ferris, R.K., Downs, R.M., Kinsey, S.T., Baumgarner, B.L., 2014. Caffeine promotes autophagy in skeletal muscle cells by increasing the calcium-dependent activation of AMP-activated protein kinase. Biochem. Biophys. Res. Commun. 453, 411–418.

Meng, F.K., Sun, H.Y., Tan, X.Y., Li, C.R., Zhou, J.F., Liu, W.L., 2011. Negative regulation of cyclin D3 expression by transcription factor c-Ets1 in umbilical cord hematopoietic cells. Acta Pharmacol. Sin. 32, 1159–1164.

Neufeld, T.P., 2010. TOR-dependent control of autophagy: biting the hand that feeds. Curr. Opin. Cell Biol. 22, 157–168.

Oladimeji, P.O., Chen, T., 2018. PXR: more than just a master xenobiotic receptor. Mol. Pharmacol. 93, 119–127.

Panickar, K.S., Jayakumar, A.R., Rao, K.V., Norenberg, M.D., 2009. Ammonia-induced activation of p53 in cultured astrocytes: role in cell swelling and glutamate uptake. Neurochem. Int. 55, 98–105.

Prakash, C., Zuniga, B., Song, C.S., Jiang, S., Cropper, J., Park, S., Chatterjee, B., 2015.

Nuclear receptors in drug metabolism, drug response and drug interactions. Nucl. Receptor Res. 2.
Rettino, A., Rafanelli, F., Genovese, G., Goracci, M., Cifarelli, R.A., Cittadini, A., Sgambato, A., 2009. Identification of Sp1 and GC-boxes as transcriptional regulators of mouse Dag1 gene promoter. Am. J. Physiol. Cell Physiol. 297, C1113–1123.
Robbins, D., Cherian, M., Wu, J., Chen, T., 2016. Human pregnane X receptor compromises the function of p53 and promotes malignant transformation. Cell Death Discovery 2, 16023.
Rysä, J., Buler, M., Savolainen, M.J., Ruskoaho, H., Hakkola, J., Hukkanen, J., 2013. Pregnane X receptor agonists impair postprandial glucose tolerance. Clin. Pharmacol. Ther. 93, 556–563.
Schneider, J.L., Cuervo, A.M., 2014. Liver autophagy: much more than just taking out the trash. Nat. Rev. Gastroenterol. Hepatol. 11, 187–200.
Sridhar, S., Botbol, Y., Macian, F., Cuervo, A.M., 2012. Autophagy and disease: always two sides to a problem. J. Pathol. 226, 255–273.
Su, Y., Chen, Z., Yan, L., Lian, F., You, J., Wang, X., Tang, N., 2018. Optimizing combination of liver-enriched transcription factors and nuclear receptors simultaneously favors ammonia and drug metabolism in liver cells. Exp. Cell Res. 362, 504–514.
Szeliga, M., Obara-Michlewska, M., 2009. Glutamine in neoplastic cells: focus on the expression and roles of glutaminases. Neurochem. Int. 55, 71–75.
Tranah, T.H., Vijay, G.K., Ryan, J.M., Shawcross, D.L., 2013. Systemic inflammation and ammonia in hepatic encephalopathy. Metab. Brain Dis. 28, 1–5.
Wang, K., Damjanov, I., Wan, Y.J., 2010. The protective role of pregnane X receptor in lipopolysaccharide/D-galactosamine-induced acute liver injury. Lab. Invest. 90, 257–265.
Wang, Y.M., Ong, S.S., Chai, S.C., Chen, T., 2012. Role of CAR and PXR in xenobiotic sensing and metabolism. Expert Opin. Drug Metab. Toxicol. 8, 803–817.
Wang, M., Zhu, J.Y., Chen, S., Qing, Y., Wu, D., Lin, Y.M., Luo, J.Z., Han, W., Li, Y.Q., 2014a. Effects of co-treatment with sulforaphane and autophagy modulators on uridine 5'-diphospho-glucuronosyltransferase 1A isoforms and cytochrome P450 3A4 expression in Caco-2 human colon cancer cells. Oncol. Lett. 8, 2407–2416.
Wang, Q., Wang, Y., Yu, Z., Li, D., Jia, B., Li, J., Guan, K., Zhou, Y., Chen, Y., Kan, Q., 2014b. Ammonia-induced energy disorders interfere with bilirubin metabolism in hepatocytes. Arch. Biochem. Biophys. 555–556, 16–22.
Wu, Y.L., Peng, X.E., Wang, D., Chen, W.N., Lin, X., 2012. Human liver fatty acid binding protein (hFABP1) gene is regulated by liver-enriched transcription factors HNF3beta and C/EBPalpha. Biochimie 94, 384–392.
Zhou, J., Liu, M., Zhai, Y., Xie, W., 2008. The antiapoptotic role of pregnane X receptor in human colon cancer cells. Mol. Endocrinol. (Baltim., Md) 22, 868–880.